

ESTIMATION OF AXIALLY LOADED DRILLED SHAFT SETTLEMENT IN CEMENTED SOIL CONDITIONS WITH AN ARTIFICIAL NEURAL NETWORK

Kevin Stanton^{1*} and Ramin Motamed²

ABSTRACT

The presence of cemented soils pose significant challenges in drilled shaft design and may prevent accurate estimates of the service limit state if traditional analytical techniques are employed. Thus, an Artificial Neural Network (ANN) is developed and tested as an alternative method for predicting settlement induced by axial loads. Training is carried out using the results of 31 field load tests performed in Las Vegas, USA, where cemented soils are common, and an automated process is employed to determine the optimal network architecture. Ultimately, a cascaded feed-forward ANN with one hidden layer consisting of six artificial neurons produced the highest quality generalization. Ten additional load tests not included in the original training, testing, or validation datasets are reserved to evaluate performance. It is observed that the ANN produces similarly accurate estimates of load-settlement on average as compared to two more traditional t - z style approaches.

Key words: Artificial neural network, cemented soils, drilled shafts, settlement.

1. INTRODUCTION

Cemented soils are often found in arid to semi-arid regions around the world and present noteworthy challenges regarding the design of cast-in-place deep foundations. These are typically referred to as drilled shafts or cast-in-drilled-hole piles (CIDH) in the United States whereas bored piles is a more common name in Europe. The colloquial term caliche is often used in parts of the United States such as Southern Nevada and Arizona to describe cemented sandy material that can be so strong that the presence of just one shaft width thick layer may reduce settlement of an axially loaded drilled shaft by as much as 50% (Stone 2009). Despite the heavy influence of cemented materials on axial response, they are difficult to characterize using common Geotechnical Investigation (GI) techniques (*e.g.*, drilling and sampling) and, as a result, foundation engineers are often forced to accept high levels of uncertainty in predictions of the service limit state. Hence, the goal of this paper is to investigate if an Artificial Neural Network (ANN) trained with commonly available design information can improve upon traditional settlement analyses for axially loaded drilled shafts in cemented soils.

An ANN is a versatile nonlinear function approximation tool based on the biological brain. The technology is quickly gaining attention in engineering disciplines because of its ability to identify complex relationships between many different inputs and outputs, even when the contact nature between parameters is entirely unknown (Garrett 1994). This makes an ANN very well suited to map one multivariate space to another given noisy or

incomplete datasets, which are common in geotechnical engineering. In general, topics for which ANN technology has been applied within the field of geotechnical engineering include, but are not limited to: Constitutive modeling (Ellis *et al.* 1995; Millar *et al.* 1995; Zhu *et al.* 1998; Penumadu and Zhao 1999; Sidarta and Ghaboussi 1998); estimation of geomaterial properties (Ellis *et al.* 1995; Najjar *et al.* 1996; Ozer *et al.* 2008; Park *et al.* 2009; Park and Kim 2011); slope stability (Ni *et al.* 1996; Neaupane and Achet 2004; Zhao 2008; Cho 2009); liquefaction (Ali and Najjar 1998; Goh 2002; Javadi *et al.* 2006); shallow foundations (Sivakugan *et al.* 1998; Provenzano *et al.* 2004; Shahin *et al.* 2005; Padmini *et al.* 2008); and deep foundations (Nawari *et al.* 1999; Teh *et al.* 1997; Kiefa 1998; Chan *et al.* 1995; Goh 1996; Das and Basudhar 2006; Park and Cho 2010).

Regarding ANN usage for deep foundations, most research either focuses on the prediction of nominal capacity directly or the complete load-settlement behavior of foundation elements. The latter, which is the topic of this study, is mainly limited to studies involving driven piles. One noteworthy example of this comes from Nejad *et al.* (2009). They employed approximately 100 sets of pile driving data to train an ANN to predict driven pile settlement given axial load and concluded that the ANN was capable of providing more accurate predictions than the other approaches considered, the t - z method and three closed form solutions from Das (1995, Poulos and Davis (1980) and Vesic (1977)). Another pertinent study, Momeni *et al.* (2015), used a feed forward ANN trained with back-propagation to estimate side and tip resistances of concrete piles given 36 sets of Pile Driving Analyzer (PDA) data, pile geometry characteristics, and Standard Penetration Test (SPT) blow counts. In this case, it was found that the ANN was able to produce accurate estimates of skin friction, end-bearing, and ultimate resistance for new test cases associated with similar soil conditions.

In this study, an automated process is carried out to determine the ideal network architecture for predicting the load-settlement response of axially loaded drilled shafts. To address the

Manuscript received September 20, 2016; revised March 10, 2017; accepted March 10, 2017.

¹ Research Associate (corresponding author), Dept. of Civil Engineering, University of Nevada, 1664 N. Virginia St., Reno, NV 89557-0258, USA (e-mail: kevinstanton@nevada.unr.edu).

² Assistant Professor, Dept. of Civil Engineering, University of Nevada, 1664 N. Virginia St., Reno, NV 89557-0258, USA.

specific issue of cemented soils, training data is taken from the Las Vegas Valley, where caliche is prevalent. The finalized ANN is selected through a semi-automated selection process based on performance metrics of many candidate networks. Prediction quality is evaluated by employing the ANN to predict the response of 10 test shafts which were not included in the original training dataset and the results are compared to those obtained with two different t - z style analyses.

2. LOAD TEST AND GI DATA

The load test and GI data required to train and evaluate the ANN is taken from the Nevada Deep Foundation Load Test Database (NDFLTD) (Motamed *et al.* 2016), which currently represents the largest collection of field load test data from Las Vegas, Nevada. It includes 41 load tests and associated GI information. In the 31 load tests that make up the training dataset for this study, shaft diameters (D) range from 0.61 to 2.44 m with embedded lengths (L) from 9.63 to 39.01 m. Figure 1 shows the approximate locations of the test shafts.

All but one of the load tests utilized a bi-directional load cell to induce movement. For these cases, the equivalent top-down curves are estimated following the methods described in Lee and Park (2008). Essentially, this involves summing the vertical loads associated with equal upward and downward movements measured during the test. Then, the theoretical elastic compression that would have been observed in a top-down test in the section of the shaft above the load cell is accounted for by considering the pattern of developed side shear and the stiffness characteristics of the constructed shaft.

In general, the available GI data for the test shafts in this study is very limited. Since the information which can be considered by the ANN must be available for all of the training data points, this means that the inputs must be kept relatively simple. In addition, the lack of site-specific laboratory test data limits the potential for existing t - z style analyses to produce accurate results in many cases. It is also difficult to obtain high quality load test data in Las Vegas with a bi-directional load test since the stiff soils tend to severely limit the movement induced either above or below the load cell. Thus, to gain insight regarding the impact of data quality, a scoring system proposed by Motamed *et al.* (2016) is employed to quantify the quality of each load test and associated GI. In general, higher GI scores are given for more thorough boring logs and available quantitative data (*i.e.*, from laboratory and/or field measurements). Particularly, the availability of a complete SPT profile and useful laboratory test data is ideal. For the load tests, scores are mainly awarded based on how close the test comes to achieving geotechnical failure. Failure is defined as the onset of plunging (movement with no additional load) or a shaft head displacement equal to 5% of D , whichever comes first. The distribution of data scores is shown in Fig. 2 and the scoring criteria is presented in Table 1.

The 10 load test data points employed for evaluation are chosen such that the predictor variables fall within the ranges encompassed by the training dataset. For example, the shaft diameters among the evaluation dataset are all greater than 0.61 m (the min of the training dataset) and less than 2.44 m (the max of the training dataset). A summary of the training and evaluation test shafts (hereafter referred to as ETS n , where n is the unique identification), are given in Tables 2 and 3, respectively. Also, the GI

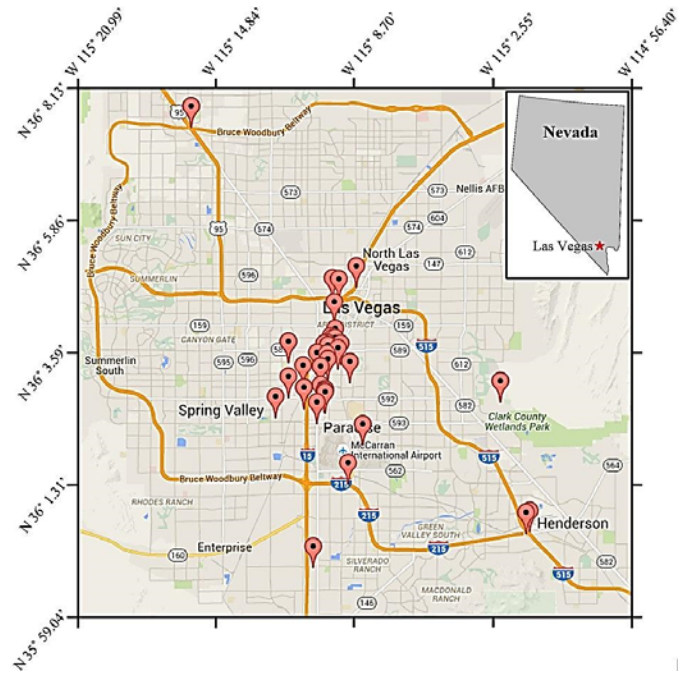


Fig. 1 Approximate locations of the test shafts included in the study

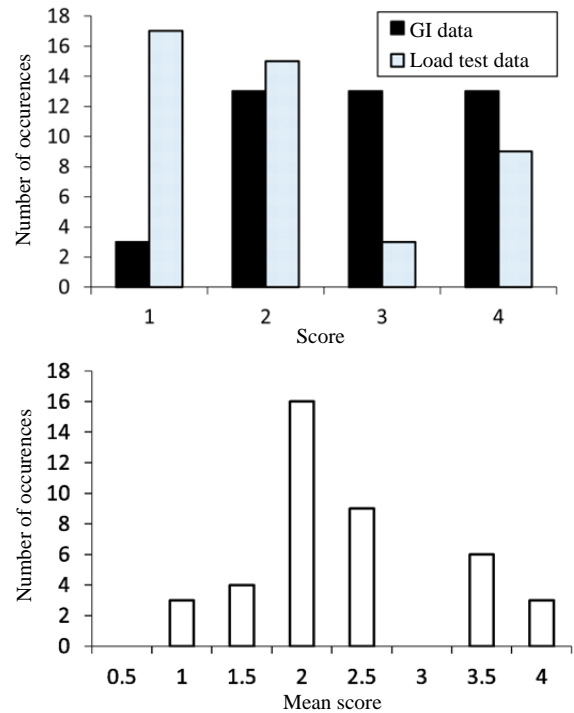


Fig. 2 Load test and GI quality scores for the data included in this study

data for each of the evaluation test shafts is given in Tables 4 through 13. For brevity, detailed GI information for the training dataset is not included herein but is available upon request. The distribution of shaft diameters, embedded lengths, and relative material fractions along the embedded shaft lengths included in the training dataset are illustrated in Fig. 3.

Table 1 Scoring criteria for load test and GI data quality

Score	Scoring criteria	
	Load test data	Geotechnical investigation data
1 (worst)	Extrapolation > 2% of the shaft diameter is required for both components of bidirectional movement or > 3% is required for a top-down test.	Incomplete boring logs with little to no SPT data or proper visual-manual classifications. No lab data.
2	Extrapolation > 2% of the shaft diameter is required for one component of bi-directional movement (second component may require < 2%) or > 2.5% but ≤ 3% is required for a top-down test.	Boring logs with minimal SPT data (<i>i.e.</i> , missing for some geologic units) and useful visual- manual classifications. No lab data.
3	Extrapolation < 2% of the shaft diameter is required for both components of bi-directional movement or > 2% but ≤ 2.5% is required for a top-down test.	Boring logs are complete with SPT data, visual-manual classification and possibly torvane or pocket pen data. Limited lab data and/or additional in situ data is available.
4 (best)	Either no extrapolation is needed or extrapolation ≤ 2% of the shaft diameter is required for only one component of load-cell movement or in total for a top-down test.	Complete boring logs with detailed material classifications, SPT data and possibly other data such as CPT or shear wave velocity measurements. Thorough lab data covering soil strengths is available.

Note: If a test shaft is not fully instrumented, the load test data score is reduced by 1. For every 45 m a borehole is spaced from the test shaft, or if the distance is unknown, the GI data score is reduced by 1. If quality control is lacking or significant problems/irregularities are present in the constructed shaft, the load test data score is reduced by 2.

Table 2 Summary of test shaft data employed for training the ANN

No.	Data score			Tip material	L (m)	D (m)	Relative fraction (%)		
	Load test	GI	Mean				Caliche	Cohesionless	Cohesive
1	2	2	2	Sand	12.2	1.5	0.00	15.01	84.99
2	4	4	4	Sand	22.7	2.3	0.00	100.00	0.00
3	1	4	2.5	Sand	9.8	2.4	23.44	50.00	26.56
4	3	4	3.5	Clay	9.6	0.6	11.71	33.23	55.06
5	3	4	3.5	Clay	25.1	0.6	12.24	13.33	74.42
6	1	2	1.5	Sand	13.1	0.6	3.49	68.60	27.91
7	1	4	2.5	Caliche	32.3	1.2	35.38	26.42	38.21
8	1	2	1.5	Caliche	32.0	1.2	57.14	19.52	23.33
9	2	2	2	Clay	35.6	1.2	5.14	28.94	65.92
10	2	2	2	Clay	34.3	1.2	8.00	8.44	83.56
11	2	2	2	Clay	37.3	1.2	13.47	19.59	66.94
12	2	3	2.5	Clay	31.1	0.9	7.35	40.20	52.45
13	1	3	2	Clay	30.5	1.2	5.50	44.00	50.50
14	1	4	2.5	Clay	30.8	1.2	8.91	35.64	55.45
15	1	4	2.5	Clay	37.2	1.8	6.15	55.33	38.52
16	3	4	3.5	Clay	37.1	1.2	10.39	15.41	74.20
17	2	2	2	Clay	27.6	1.1	22.60	49.61	22.78
18	1	3	2	Caliche	32.2	1.1	32.70	34.60	32.70
19	1	3	2	Sand	39.0	1.2	20.90	36.52	42.58
20	1	2	1.5	Caliche	34.1	1.2	20.04	38.34	41.61
21	2	2	2	Clay	25.0	1.2	4.88	0.00	95.12
22	1	4	2.5	Clay	27.6	1.2	2.76	17.13	80.11
23	4	4	4	Clay	29.1	1.5	5.24	23.87	70.89
24	4	3	3.5	Clay	18.9	1.2	18.55	20.16	61.29
25	1	3	2	Sand	30.9	1.2	4.48	36.72	58.81
26	1	3	2	Clay	34.4	1.8	3.99	34.69	61.31
27	2	2	2	Caliche	31.8	1.1	13.42	26.20	60.39
28	4	4	4	Sand	22.9	1.1	13.33	62.00	24.67
29	4	1	2.5	Clay	34.1	1.1	8.04	11.16	80.80
30	1	3	2	Clay	32.4	1.2	4.24	36.16	59.60
31	4	4	4	Caliche	25.6	1.2	0.60	17.26	82.14

Table 3 Summary of evaluation test shaft data

ETS _n	Data score			Tip material	L (m)	D (m)	Relative fraction (%)		
	Load test	GI	Mean				Caliche	Cohesionless	Cohesive
1	2	2	2	Sand	31.4	1.2	12.6	55.8	31.6
2	2	3	2.5	Caliche	37.5	1.2	12.2	39.8	48.0
3	2	2	2	Sand	37.1	1.2	9.4	48.2	42.4
4	1	3	2	Sand	30.5	1.1	47.5	10.5	42.0
5	4	3	3.5	Clay	29.3	1.5	5.2	23.8	71.0
6	4	3	3.5	Clay	21.3	1.1	6.4	38.6	55.0
7	2	2	2	Caliche	21.3	1.1	27.9	12.8	59.4
8	2	3	2.5	Caliche	32.2	1.1	29.9	37.4	32.7
9	2	2	2	Sand	30.8	1.5	0.0	97.5	2.5
10	4	4	4	Caliche	25.3	0.9	0.6	16.3	83.1

Table 4 Idealized stratigraphy and material properties for ETS1 (water table depth = 25.8 m)

Base layer depth (m)	Soil type	γ (kN/m ³)	ϕ (deg)	N_{SPT}	s_u (kPa)
1.2	Cohesionless (SM)	15.4	43	25	–
2.4	Cohesive	17.4	–	19	143
3.5	Cohesionless (GP)	17.3	43	39	–
4.1	Cohesive	17.4	–	45	261
5.0	Caliche	22.0	40	–	–
5.5	Cohesive	17.4	–	45	245
6.7	Caliche	22.0	40	–	–
8.2	Cohesionless (SM)	15.9	40	21	–
9.1	Cohesionless (SM)	18.4	44	50	–
11.1	Caliche	22.0	40	–	–
12.8	Cohesive	18.7	–	6	34
17.4	Cohesionless (SM)	17.9	38	15	–
18.3	Cohesive	20.6	–	50	230
18.9	Caliche	22.0	40	–	–
19.7	Cohesionless (SM)	18.7	41	30	–
19.8	Cohesive	20.6	–	24	107
20.7	Cohesionless (SM)	18.7	41	30	–
21.2	Caliche	22.0	40	–	–
25.8	Cohesive	20.5	–	19	78
26.2	Cohesive	20.6	–	40	158
27.4	Cohesionless (SM)	17.0	36	11	–
29.6	Cohesive	20.2	–	20	77
30.6	Cohesionless (SM)	16.6	36	10	–
37.2	Cohesionless (SM)	18.2	39	25	–

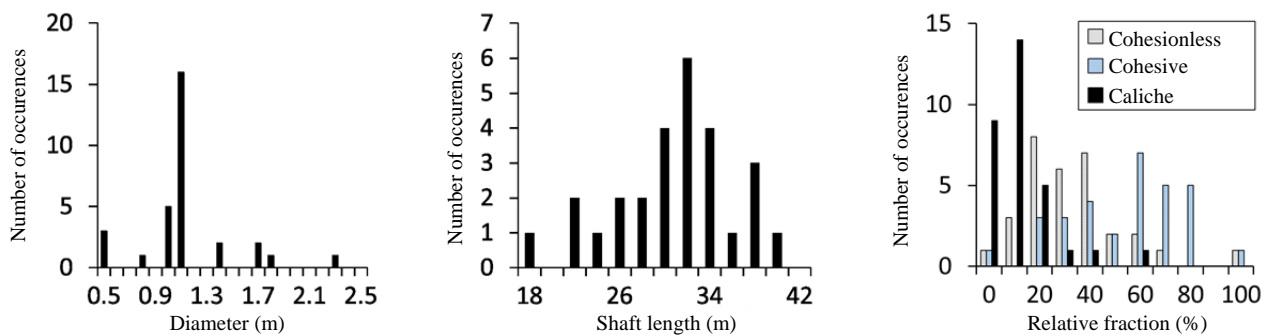


Fig. 3 Distribution of select predictor variables in the training dataset

Table 5 Idealized stratigraphy and material properties for ETS2 (water table depth = 5.6 m)

Base layer depth (m)	Soil type	γ (kN/m ³)	ϕ (deg)	N_{SPT}	s_u (kPa)
0.5	Cohesionless (SP)	18.4	43	25	–
2.4	Cohesive	17.4	–	50	448
3.7	Cohesionless (SP)	17.1	40	21	–
4.1	Cohesive	17.4	–	40	237
4.6	Cohesionless (GP)	17.6	43	40	–
5.6	Cohesionless (SM)	22.0	44	50	–
6.1	Cohesive	20.6	–	40	239
7.9	Cohesionless (SM)	21.2	44	44	–
10.1	Cohesive	20.6	–	31	212
11.7	Cohesionless (GP)	22.0	44	50	–
11.9	Cohesive	20.6	–	40	253
12.3	Cohesionless (GP)	22.0	44	50	–
12.6	Caliche	22.0	40	–	–
13.1	Cohesionless (GP)	20.3	43	40	–
13.7	Caliche	22.0	40	–	–
14.6	Cohesionless (SM)	21.7	44	50	–
14.9	Cohesive	20.6	–	35	201
16.6	Cohesionless (SM)	19.8	42	37	–
18.1	Cohesive	20.5	–	24	130
18.6	Caliche	22.0	40	–	–
19.2	Cohesive	20.6	–	30	156
19.5	Cohesionless (SM)	19.8	42	40	–
20.1	Cohesive	20.6	–	45	230
24.2	Cohesionless (SM)	20.4	43	50	–
26.5	Cohesive	20.5	–	38	179
27.3	Cohesionless (SM)	18.9	41	33	–
29.7	Cohesive	20.6	–	31	134
30.0	Cohesionless (GP)	19.2	42	40	–
30.5	Cohesive	20.6	–	23	98
31.4	Caliche	22.0	40	–	–
33.5	Cohesive	20.6	–	50	204
34.6	Cohesionless (SM)	19.2	42	43	–
35.7	Cohesive	20.3	–	18	72
36.1	Cohesionless (GP)	18.2	39	25	–
36.6	Cohesive	20.4	–	30	118
38.1	Caliche	22.0	40	–	–
40.5	Cohesive	20.6	–	49	188
41.3	Caliche	22.0	40	–	–

Table 6 Idealized stratigraphy and material properties for ETS3 (water table depth = 4.6 m)

Base layer depth (m)	Soil type	γ (kN/m ³)	ϕ (deg)	N_{SPT}	s_u (kPa)
16.5	Cohesionless (SP)	22.0	45	50	–
17.2	Caliche	22.0	40	–	–
18.3	Cohesive	20.6	–	48	264
20.4	Cohesionless (SM)	19.0	41	30	–
20.8	Caliche	22.0	40	–	–
21.9	Cohesive	18.9	–	7	36
22.3	Cohesionless (SM)	18.5	40	25	–
23.2	Cohesive	19.3	–	10	50
23.8	Cohesionless (SM)	19.5	42	39	–
28.0	Cohesive	20.6	–	30	142
28.4	Caliche	22.0	40	–	–
29.6	Cohesive	20.6	–	21	94
30.3	Cohesionless (SM)	17.8	38	15	–
30.5	Caliche	22.0	40	–	–
31.9	Cohesive	20.6	–	20	86
32.2	Cohesionless (SM)	18.2	39	21	–

Table 6 (Continued)

Base layer depth (m)	Soil type	γ (kN/m ³)	ϕ (deg)	N_{SPT}	s_u (kPa)
32.7	Caliche	22.0	40	–	–
34.9	Cohesive	19.6	–	15	63
35.2	Cohesionless (SM)	16.5	35	9	–
36.0	Caliche	22.0	40	–	–
37.2	Cohesive	22.0	–	45	179
37.5	Cohesionless (SM)	19.6	42	50	–
38.2	Caliche	22.0	40	–	–
39.1	Cohesive	20.6	–	45	176
40.2	Cohesive	19.0	–	10	38
41.8	Cohesionless (SM)	19.5	42	50	–
53.6	Cohesionless (SM)	15.7	34	8	–

Table 7 Idealized stratigraphy and material properties for ETS4 (water table depth = 7.3 m)

Base layer depth (m)	Soil type	γ (kN/m ³)	ϕ (deg)	N_{SPT}	s_u (kPa)
3.0	Cohesionless (SM)	21.7	30	25	–
5.5	Cohesive	19.2	–	39	223
7.0	Cohesionless (SP)	21.7	44	50	–
12.6	Caliche	22.0	40	–	–
14.6	Cohesive	17.8	29	29	156
14.9	Caliche	22.0	40	–	–
15.2	Cohesive	20.6	–	20	104
16.6	Caliche	22.0	40	–	–
20.0	Cohesive	20.6	–	40	196
20.7	Cohesionless (SM)	20.3	37	13	–
23.5	Caliche	22.0	40	–	–
24.8	Cohesive	19.2	–	12	52
25.8	Caliche	22.0	40	–	–
26.1	Cohesive	20.6	–	50	213
27.7	Caliche	22.0	40	–	–
30.3	Cohesive	20.4	–	50	203
30.6	Caliche	22.0	40	–	–
31.1	Cohesive	19.8	–	15	59
32.6	Caliche	22.0	40	–	–
33.5	Cohesionless (SM)	20.1	37	16	–

Table 8 Idealized stratigraphy and material properties for ETS5 (water table depth = 24.7 m)

Base layer depth (m)	Soil type	γ (kN/m ³)	ϕ (deg)	N_{SPT}	s_u (kPa)
4.3	Cohesive	17.4	–	28	219
5.1	Cohesionless (SM)	17.1	43	36	–
5.8	Cohesionless (GP)	18.7	44	50	–
6.6	Cohesionless (SM)	22.0	44	50	–
7.3	Cohesionless (GP)	20.3	44	49	–
7.5	Cohesive	17.4	–	50	314
7.9	Cohesionless (SM)	16.7	42	32	–
8.4	Cohesive	17.4	–	35	210
9.1	Cohesionless (SM)	18.2	44	50	–
11.9	Cohesive	17.4	–	39	228
12.3	Cohesionless (GP)	16.3	42	31	–
13.3	Cohesive	17.4	–	48	254
14.6	Cohesive	17.4	–	35	179
15.1	Cohesionless (GP)	16.0	41	31	–
15.5	Cohesive	17.4	–	44	215
16.0	Cohesionless (GP)	15.6	39	20	–
17.4	Cohesionless (GP)	17.1	43	49	–
18.9	Caliche	22.0	40	–	–
30.5	Cohesive	20.5	–	40	161

Table 9 Idealized stratigraphy and material properties for ETS6 (water table depth = 6.1 m)

Base layer depth (m)	Soil type	γ (kN/m ³)	ϕ (deg)	N_{SPT}	s_u (kPa)
0.6	Cohesionless (SP)	21.4	44	35	–
1.8	Cohesionless (SM)	22.0	45	50	–
3.7	Cohesionless (SP)	20.0	44	50	–
6.1	Cohesionless (SM)	18.2	44	50	–
7.6	Cohesionless (SM)	22.0	44	50	–
8.4	Cohesive	20.6	–	35	212
9.1	Cohesionless (SP)	22.0	44	50	–
11.9	Cohesionless (SM)	21.2	39	50	–
13.7	Cohesive	20.6	–	33	189
15.1	Caliche	20.4	40	–	–
23.3	Cohesive	20.6	–	36	175
23.5	Cohesionless (SP)	21.7	43	50	–
24.4	Cohesive	20.6	–	45	204

Table 10 Idealized stratigraphy and material properties for ETS7 (water table depth = 6.4 m)

Base layer depth (m)	Soil type	γ (kN/m ³)	ϕ (deg)	N_{SPT}	s_u (kPa)
1.1	Cohesionless (SP)	23.9	45	50	–
2.6	Cohesionless (SM)	16.5	42	25	–
3.4	Caliche	22.0	40	–	–
4.0	Cohesive	17.4	–	25	135
5.8	Cohesionless (SM)	21.5	43	41	–
6.4	Caliche	22.0	40	–	–
10.7	Cohesive	19.6	–	36	224
12.2	Cohesionless (SM)	18.4	42	28	–
12.6	Caliche	22.0	40	–	–
18.6	Cohesive	20.0	–	46	253
20.3	Caliche	22.0	40	–	–
25.8	Cohesive	20.6	–	50	236
26.2	Cohesionless (SM)	18.2	38	16	–
27.4	Cohesive	20.6	–	25	110
27.7	Cohesionless (SM)	19.6	42	40	–
29.6	Caliche	22.0	40	–	–
30.0	Cohesive	20.6	–	45	189
30.8	Caliche	22.0	40	–	–
31.4	Cohesive	20.6	–	45	185
32.0	Caliche	22.0	40	–	–

Table 11 Idealized stratigraphy and material properties for ETS8 (water table depth = 5.3 m)

Base layer depth (m)	Soil type	γ (kN/m ³)	ϕ (deg)	N_{SPT}	s_u (kPa)
1.5	Cohesionless (SM)	20.7	12	19	–
3.8	Cohesive	20.1	–	10	59
5.8	Cohesionless (SM)	21.2	43	41	–
7.0	Cohesionless (SP)	22.0	44	50	–
9.1	Caliche	22.0	40	–	–
10.2	Cohesionless (SM)	23.2	44	50	–
11.6	Caliche	22.0	40	–	–
13.0	Cohesive	20.6	–	42	250
14.5	Cohesionless (SM)	21.4	39	14	–
16.0	Cohesionless (GP)	18.5	41	24	–
17.1	Cohesionless (SM)	22.9	43	50	–
18.0	Caliche	22.0	40	–	–
22.1	Cohesive	19.8	–	12	60
23.2	Cohesionless (SM)	20.6	38	50	–
23.6	Caliche	22.0	40	–	–
26.2	Cohesionless (SM)	18.7	41	30	–
26.5	Caliche	22.0	40	–	–
28.7	Cohesive	17.9	–	31	135
29.1	Caliche	22.0	40	–	–
30.2	Cohesive	20.6	–	40	169
30.8	Caliche	22.0	40	–	–
31.9	Cohesive	20.6	–	40	165
35.2	Caliche	22.0	40	–	–

Table 12 Idealized stratigraphy and material properties for ETS9 (water table depth = 5.6 m)

Base layer depth (m)	Soil type	γ (kN/m ³)	ϕ (deg)	N_{SPT}	s_u (kPa)
0.5	Cohesionless (GP)	19.9	44	35	–
0.9	Cohesionless (SM)	18.7	41	17	–
1.5	Cohesive	17.4	–	50	451
2.0	Caliche	22.0	40	–	–
3.8	Cohesive	17.4	–	29	179
7.9	Cohesionless (SM)	20.2	43	37	–
8.7	Cohesionless (SP)	22.0	44	50	–
10.7	Cohesionless (SM)	18.9	44	50	–
11.1	Cohesionless (SP)	22.0	44	50	–
12.2	Cohesionless (SM)	19.8	42	33	–
13.0	Cohesive	20.6	–	33	206
15.8	Cohesionless (SM)	21.2	44	48	–
17.7	Cohesionless (SM)	19.2	41	30	–
35.4	Cohesionless (SM)	19.3	42	40	–

Table 13 Idealized stratigraphy and material properties for ETS10 (water table depth = 4.9 m)

Base layer depth (m)	Soil type	γ (kN/m ³)	ϕ (deg)	N_{SPT}	s_u (kPa)
4.9	Cohesive	19.5	–	18	95
10.1	Cohesive	18.0	–	11	58
14.9	Cohesive	18.8	–	36	192
16.8	Cohesionless (SM)	19.5	42	30	–
18.3	Cohesionless (GP)	21.7	44	50	–
20.7	Cohesive	19.8	–	19	117
24.4	Cohesive	20.1	–	40	83
25.1	Cohesionless (GP)	19.8	43	50	–
25.3	Caliche	22.0	40	–	–

3. ANN ARCHITECTURE AND TRAINING

The types of problems an ANN is best suited to handle are dictated by the training data and architecture employed. The ideal network architecture and content/format of the training data are also interdependent, making it difficult to determine the optimal setup for an ANN. For this study, various organizations of training data were tested by optimizing feed-forward and cascaded feed-forward Multi-Layer Perceptron (MLP) architectures in an automated fashion as described hereafter.

In total, 31 data points are used for training and an additional 10 are reserved for evaluations through blind predictions. The prescribed outcomes for each input sample consist of the measured downward movement associated with a given value of top load applied to the shaft head. Therefore, many input samples of top load are required to properly capture the load-settlement response for each set of load test data. The tipping materials are interpreted by the computer as follows: 1 = sand, 2 = clay, 3 = caliche. It should be noted that there was insufficient data regarding shafts tipped into Partially Cemented Material (PCM) to properly train the ANN to deal with such cases. Additionally, the relative fraction of PCM is defined independently of the values entered for the associated parent materials. For example, if partially cemented clay was noted in a boring log, then the relative fraction entered for cohesive material would include the partially cemented clay as well. Hence, the sum of the relative fractions for cohesive, cohesionless, and caliche always equate to 100% whether or not any partial cementation was evident.

Standard Penetration Test (SPT) data is the only form of in-situ test data that is available for all of the data in the NDFLTD and is therefore employed to help characterize the soil profile. Prelimi-

nary experiments in which raw SPT blow counts (N_{SPT}), counts corrected for hammer efficiency (N_{60}), and counts further corrected for overburden pressure (N_{160}) revealed that using N_{160} produced poorer generalization compared to using N_{SPT} or N_{60} with the water table defined separately. Hence, in contrast with recommendations from Nejad *et al.* (2009) that the depth of the water table is best captured by N_{160} , N_{SPT} is used herein to characterize the subsurface along with the other aforementioned parameters. This is accomplished by dividing the embedded shaft length into 20 parts (*i.e.*, increments of 5%) and presenting the network with the mean N_{SPT} measured over each. The final input structure for the ANN is shown in Table 14.

Presently, the most common training mechanism for feed-forward ANNs is back-propagation and the traditional implementation of back-propagation uses what is known as a gradient descent algorithm to adjust the weights during training (Rumelhart *et al.* 1988). However, this method of optimization tends to converge slowly and is prone to incorrectly converging on local minima (Lahmiri 2011). Thus, the task of adjusting weights and thresholds during back-propagation in this study is carried out with the Levenberg-Marquardt algorithm (Marquardt 1963; Levenberg 1944). This approach has been shown to improve generalization in most cases and typically takes less time to run than other similar algorithms such as Bayesian regularization (Jeffreys 1939). The update rule of the Levenberg-Marquardt algorithm is described by Eq. (1)

$$W_{k+1} = W_k - (J_k^T J_k + \mu I)^{-1} J_k e_k \quad (1)$$

where W_k is the current weight, W_{k+1} is the next weight, J is the Jacobian matrix, μ is a positive value known as the combination coefficient, I is the identity matrix, and e is the error vector.

Table 14 Structure of training/input data used for the ANN in this study

Inputs											Output
Top load (kN)	Shaft top (m)	L^a (m)	Cohesionless frac. (%)	Cohesive frac. (%)	Caliche frac. (%)	PCM ^b frac. (%)	Water table (m)	Tip mat.	D^c (m)	N_{SPT}^d per 5% of L	Disp. (cm)

a Embedded shaft length

b Partially cemented material

c Shaft diameter

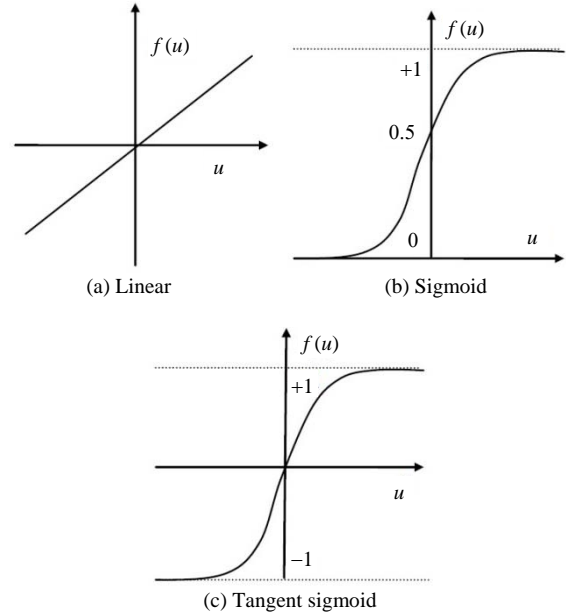
d Consists of 20 individual inputs (*i.e.*, average over 0 ~ 5%, 5 ~ 10%, 10 ~ 15%, 15 ~ 20%, etc.)

Training is performed using the “cascadeforwardnet” and “feedforwardnet” functions in Matlab (Matlab 2014) for cascaded and traditional architectures, respectively. These require the input-target pairs to be sorted into three categories: Training, validation, and testing. Training data is presented to the network during training so that adjustments can be made to minimize error. Validation data is used to measure network generalization and stop the training process when generalization stops improving (*i.e.*, these points directly affect training). Testing points, on the other hand, have no effect on training so as to provide an independent measure of performance after training is complete. That being said, for this study, the load-settlement pairs in the initial testing dataset all conform to the same general trends that the network sees during training. It is therefore necessary to perform a more rigorous evaluation of the ANN by comparing to entirely new and complete load-settlement datasets. Thus, the metrics associated with the testing dataset are only considered to aid in the selection of the finalized ANN in this research. The following steps outline the development, training, and selection of the finalized ANN:

1. Collect input data and organize into an array where each row contains the elements shown in Table 14.
2. Interpret measured load test data to define a column vector of target displacements associated with each prescribed value of top-load.
3. Systematically train multiple candidate networks, each with a different number of hidden layers and neurons. This is performed for both feed-forward and cascaded feed-forward architectures considering all possible permutations of tangent sigmoid, logarithmic sigmoid, and linear activation functions applied to the hidden and output layers.
 - 70% of samples are used for training, 15% for validation, and 15% for testing (ratios determined through trial and error).
 - Assign data to each category with the interlaced division function in Mat-lab (divint) to ensure that all magnitudes of load and settlement are equally represented.
 - Training is carried out with the Levenberg-Marquardt algorithm.
 - The linear, logarithmic sigmoid, and tangent sigmoid activation functions are described by Eqs. (2) ~ (4), respectively. These are also illustrated in Fig. 4.

$$f(u) = \alpha u \quad (2)$$

$$f(u) = \frac{1}{1 + e^{-\alpha u}}, \quad 0 \leq f(u) \leq 1 \quad (3)$$


Fig. 4 Activation functions used in artificial neurons

$$f(u) = \frac{2}{1 + e^{-\alpha u}} - 1, \quad -1 \leq f(u) \leq 1 \quad (4)$$

4. Determine the optimal architecture by programmatically filtering out trained ANNs based on performance indicated by the correlation coefficient and Mean Squared Error (MSE) between the predicted and target outcomes.
 - Qualitative inspections are performed for the top ten out of 1×10^7 trained networks for to ensure that physically reasonable predictions are obtained in as many cases as possible.

The finalized ANN employs cascaded feed-forward architecture with a single hidden layer consisting of 6 neurons, though the optimal number of neurons in the hidden layer would have been ≈ 31 if cascaded architecture was not used. The greater number of connections in the cascaded networks, however, enables smaller hidden layers to produce the best generalizations for the data in this study. It is important to note that the optimal number of hidden layers is found to be one regardless of other architectural characteristics. This supports the findings from Hornik *et al.* (1989) which suggest that any continuous function can be approximated with a single layer, feed-forward ANN.

Figure 5 portrays the finalized ANN architecture. In this cascaded framework, there is a connection between the inputs and all subsequent weights (w) and biases (b). While a tangent sigmoid activation function is selected for the hidden layer, a logarithmic sigmoid is employed in the output layer to avoid prediction of negative settlement values. This works for any combination of inputs because the result of the logarithmic sigmoid function always ranges between 0 and 1 (as opposed to -1 and 1 for linear or tangent sigmoid). A more complex alternative to this approach might involve the application non-classical logic (*i.e.*, fuzzy logic) (Zadeh 1965) to create what is known as a neuro-fuzzy inference system. In theory, such a system could lead to improved generalization but in order to quantify any potential benefits, it is necessary to first understand how the network performs using purely classical logic. Hence, the decision to use a logarithmic sigmoid activation function in the output layer is advantageous because it enables physically reasonable predictions within the framework of a classical ANN.

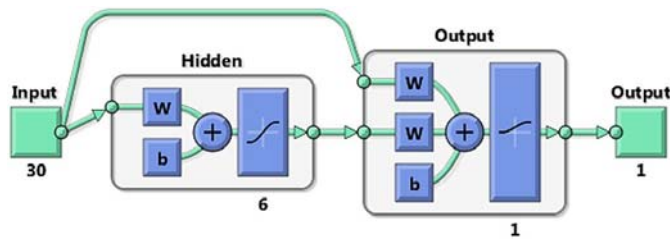


Fig. 5 Finalized ANN architecture

A histogram of the error for all instances of training, testing, and validation is shown in Fig. 6. In general, this describes how well the trained ANN predicts target values based on inputs included in the original training dataset. The lack of instances with large errors indicates that the ANN would produce reasonably accurate results if presented with any of the original inputs.

Performance regressions for training, testing, and validation are given in Fig. 7. These plots suggest that the ANN achieves strong generalization among the 31 load tests in the training dataset, although they do not give any information pertinent to how the network might perform if presented with entirely new data.

The progression of validation performance, quantified by the MSE, is shown in Fig. 8.

This reveals that optimum performance was reached at epoch 65 with an MSE of 0.033755.

4. TRADITIONAL ANALYTICAL TECHNIQUES

In order to benchmark the ANN, *t-z* style analyses are carried out using the programs SHAFT (Reese *et al.* 2012) and CGI-DFSAP (Norris 1986; Ashour *et al.* 1998) to estimate the load-settlement response of the evaluation test shafts described in Table 3.

Since drilled shafts in Las Vegas soil conditions often derive a significant portion of their resistance from both skin friction and end bearing, the analyses carried out in SHAFT and CGI-DFSAP attempt to capture the contribution of both. The load transfer curves in SHAFT for frictional and tip resistance are based on the results of field load tests conducted on drilled shafts with diameters ranging from 0.6 to 0.9 m (Reese and O’Neill 1988) while those in CGI-DFSAP are based on the work of Ashour and Helal (2012) for cohesive material/rock and Ashour *et al.* (2010) for cohesionless material.

Very little site specific strength data is available for cemented materials associated with the test shafts in this study. Thus, in both SHAFT and CGI-DFSAP, cemented layers (*i.e.*, caliche) are modeled as weak rock (O’Neill *et al.* 1996) with an unconfined compressive strength of 29.9 MPa, effective friction angle of 40°, and a total unit weight of 22 kN/m³. Laboratory test data from in Western Technologies Inc. (1994), Arup (2011), and Rinne *et al.* (1996) suggest that these numbers represent the most typical values encountered for caliche in the Las Vegas area. Also, CGI-DFSAP allows the user to specify the strain at 50% axial strain, E_{50} , for each soil layer. For this study, the internally computed values of E_{50} are employed for sands (Norris 1986) and clays (Evans 1982). Alternatively, a value of $E_{50} = 0.001$ is applied for caliche layers based on the average from 10 triaxial compression tests performed on caliche samples from Las Vegas by Rinne *et al.* (1996).

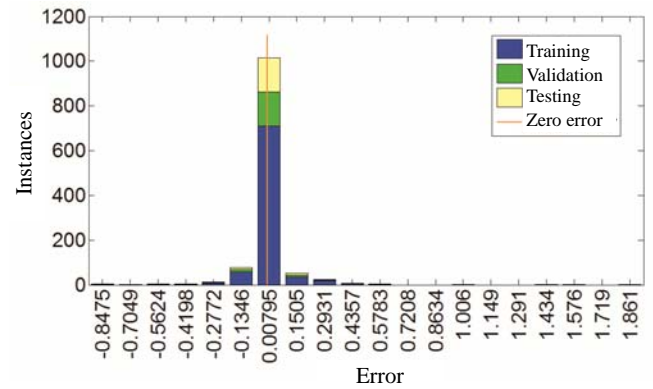


Fig. 6 Histogram of the error associated with output and target pairs (instances) in the training, validation, and testing datasets

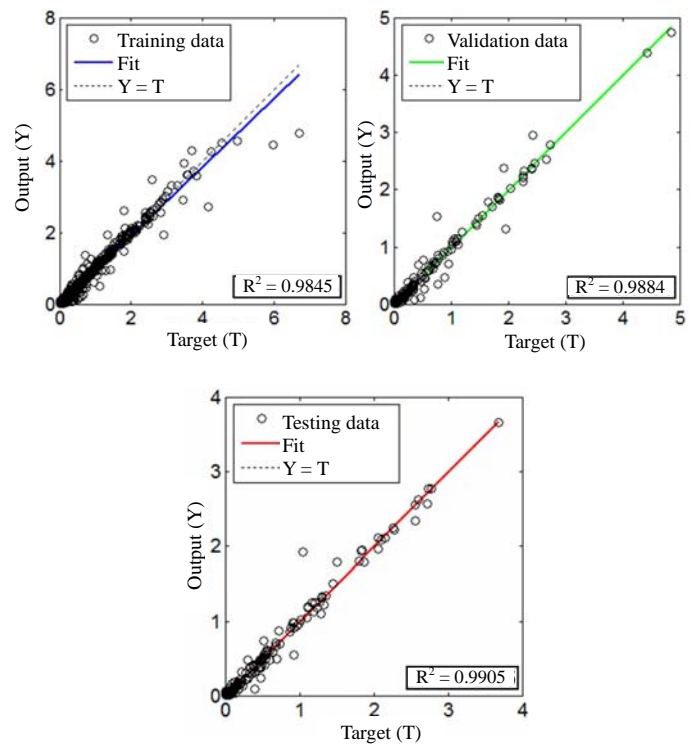


Fig. 7 ANN performance regressions for training, testing, and validation

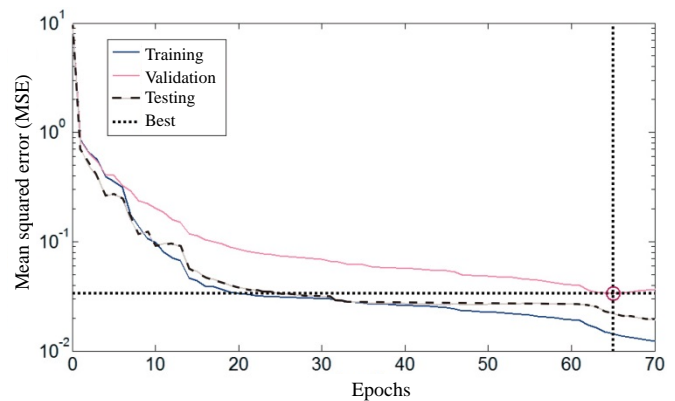


Fig. 8 Progression of ANN validation performance

5. RESULTS

The load-settlement predictions from each of the three methods considered are presented in Fig. 9 and the Root Mean Squared Errors (RMSEs) given in Table 15 quantify the overall prediction qualities. RMSE is defined by Eq. (5):

$$RMSE = \sqrt{\frac{\sum_{\delta=0}^{\delta=\delta_{max}} (Q_{measured, \delta} - Q_{predicted, \delta})^2}{n}} \quad (5)$$

where δ is the level of vertical displacement at the shaft head, Q is the axial load at the shaft head, and n is the total number of displacement levels considered.

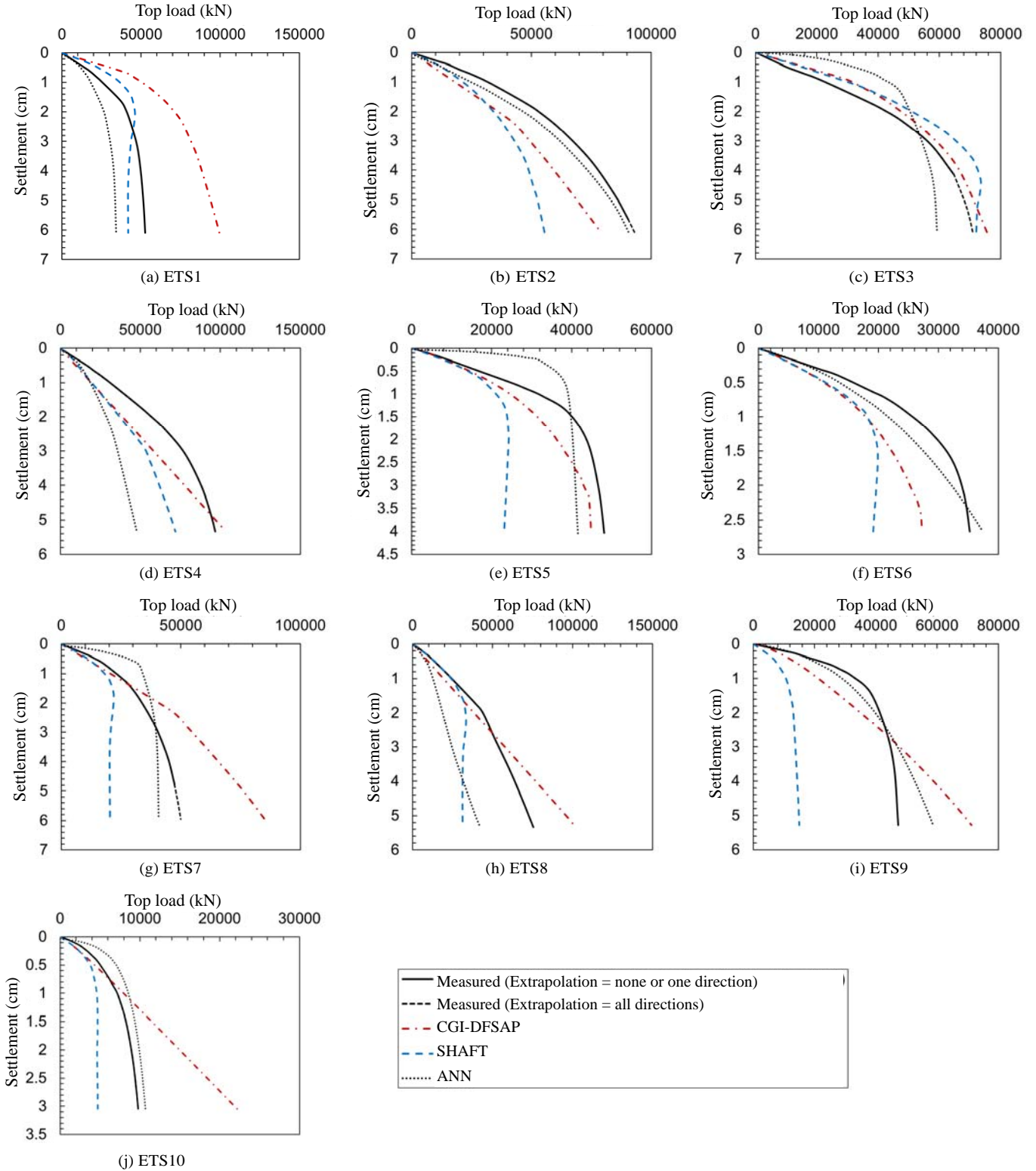


Fig. 9 Measured and predicted axial load-settlement responses for the evaluation test shafts

Table 15 RMSE for different prediction methods

ETS _n	RMSE (kN)		
	CGI-DFSAP	SHAFT	ANN
1	25247	7391	10794
2	13536	13235	5889
3	4704	7255	11591
4	12775	20616	35865
5	5240	18236	8907
6	7308	10859	2702
7	18777	19775	7043
8	11658	24379	25820
9	11625	27720	5386
10	6151	3583	1266

The plots in Fig. 9 extend to the interpreted nominal capacity of each test shaft, defined as the lesser load corresponding to the displacement equal to 5% of the shaft diameter or the onset of plunging failure (*i.e.*, displacement with no additional load). Some amount of extrapolation was required to meet this criteria for 4 of the 10 evaluation load tests.

Inspection of Fig. 9 suggests that, in general, the ANN marginally outperforms CGI-DFSAP and both the ANN and CGI-DFSAP produce more accurate settlement predictions than SHAFT. That being said, the performance of each prediction method is inconsistent.

SHAFT overestimated the measured settlements at all load levels for all evaluation test shafts except ETS1 and ETS3 (ETS1 settlement was overestimated for loads greater than approximately 40000kN). In addition, blind interpretation of the SHAFT predictions would erroneously indicate plunging failure for 6 of the 10 evaluation test shafts. In comparison, CGI-DFSAP predicted consistently stiffer responses than SHAFT and did not suffer from the tendency to predict plunging failure prematurely. The relatively stiff responses from CGI-DFSAP also represent a general improvement over those from SHAFT. While both procedures appear more accurate at low levels of displacement (*i.e.*, the elastic region), CGI-DFSAP seems to be more capable of capturing nonlinear behavior.

The impact of data quality on RMSE is described by the statistics provided in Table 16 and the illustration in Fig. 10. These confirm that the mean performance of each prediction method, indicated by the RMSE, varies for different data qualities.

According to Fig. 10, mean RMSE and data quality are positively correlated for all prediction methods. Additionally, the data given in Table 16 reveals that while the ANN produces the lowest mean RMSE in most cases, it is associated with the greatest COV for all data qualities. The difference between the minimum and maximum RMSE from the ANN is also greatest for the first two data quality bins (all data and mean score > 2) but is lower than that from SHAFT when the highest quality data is considered. In light of these observations, the ANN appears to have the potential to produce large errors in extreme cases, although its best predictions are more accurate than those from CGI-DFSAP or SHAFT.

To gain a sense for how each prediction method performs at different settlement stages, any measured responses that did not reach the $\delta/D = 5\%$ failure criteria (*i.e.*, reached plunging first were extrapolated to allow comparisons to be made for equivalent levels of displacement. Thus, Fig. 11 presents the mean

Table 16 Summary statistics of RMSE for three data quality bins

Prediction method	All data		Mean score > 2		Mean score ≥ 3	
	Mean (kN)	COV	Mean (kN)	COV	Mean (kN)	COV
SHAFT	15305	0.53	14058	0.56	10893	0.67
CGI-DFSAP	11702	0.55	8779	0.41	6233	0.17
ANN	11526	0.90	8917	1.11	4292	0.95

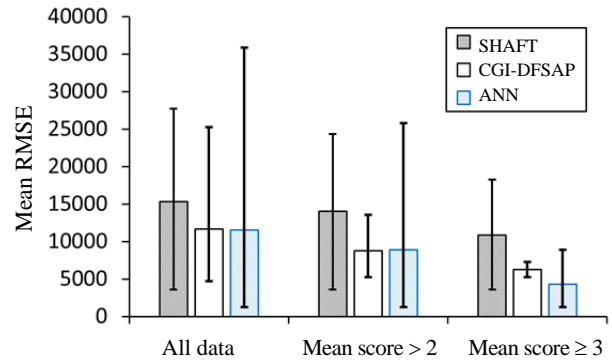


Fig. 10 Impact of data quality on prediction accuracy (error bars indicate min/max)

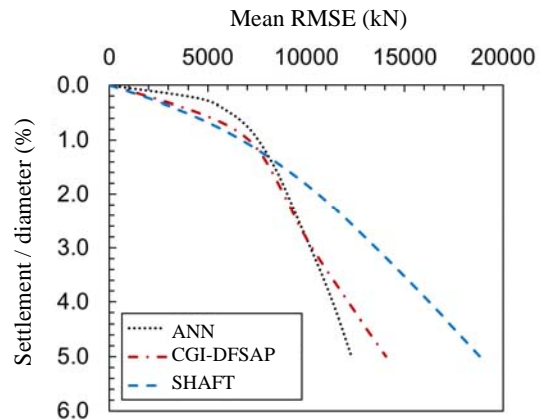


Fig. 11 Mean RMSE for all evaluation test shaft predictions for equivalent settlement stages (defined using settlement normalized by shaft diameter)

RMSE for each prediction method as a function of the settlement level normalized by the shaft diameter. Hence, for each settlement stage, the RMSE is computed up to that point for each individual load test prediction. Finally, the average RMSE across all ten predictions for comparable settlement stages is calculated to provide a single point for one of the curves in Fig. 11 and the process is repeated for increasingly large settlement stages up to $\delta/D = 5\%$ and again for each prediction method.

Figure 11 suggests that at lower settlement stages (*i.e.*, $\delta/D \leq 1\%$), the ANN tends to be less accurate than the $t-z$ style approaches, which are roughly equivalent to each other. For δ/D between 1 and 3%, the ANN and CGI-DFSAP accuracy are near-

ly equivalent and both appear to outperform SHAFT. However, at settlement stages greater than $\delta/D = 3\%$, the ANN predictions are the slightly and significantly more accurate than those from CGI-DFSAP and SHAFT, respectively.

6. CONCLUSIONS

It has been demonstrated that a cascaded feed-forward ANN trained with back-propagation (using the Levenberg-Marquardt method) can predict settlement of axially loaded drilled shafts in cemented soils with accuracy comparable to more traditional $t-z$ style analyses. Overall, despite being marginally less accurate at smaller settlement levels, the ANN achieved the lowest RMSE for five of the ten evaluation test shafts whereas CGI-DFSAP was most accurate for four cases and SHAFT was most accurate for just one case. Also, while the ANN predictions are slightly more conservative on average than those from CGI-DFSAP or SHAFT, the variation among the ANN predictions is also greater, although the variation becomes less significant for higher data qualities. Thus, there is still room for improvement.

Some noteworthy challenges which have been overcome in this study regarding the development of an ANN for the purpose of drilled shaft settlement analysis include the prevention of negative settlement predictions (without the use of fuzzy logic) and the development of a methodology for determining the ideal architecture for an ANN of this nature (*i.e.*, inputs structure, number of hidden layers/neurons, cascaded/not cascaded). The results suggest that the former issue is effectively solved with a logarithmic sigmoid activation function applied in the output layer. It is also found that the programmatic implementation of the aforementioned ANN development procedure has the potential to produce an ANN with acceptable performance, even with the relatively limited GI data available herein. This is particularly useful for cases in which strong network generalization is difficult to achieve when network configurations are determined through manual trial and error.

Any interested readers are encouraged to contact the first author to obtain a copy of the ANN developed for this paper.

ACKNOWLEDGMENTS

The authors would like to recognize the Nevada Department of Transportation for funding the data collection efforts (award number P515-13-803) and Farzan Kazemi for his support throughout this study.

REFERENCES

- Ali, H. and Najjar, Y. (1998). "Neu ronet-based approach for assessing liquefaction potential of soils." *Transportation Research Record: Journal of the Transportation Research Board*, 1633, 3–8.
- Arup (2011). *Vegas High Roller-Geotechnical Interpretive Report*. Report No. 210193, Prepared for Caesar's Entertainment.
- Ashour, M. and Helal, A. (2012). "Response of axially loaded piles in sands with and without seismically induced porewater pressures." *International Journal of Geomechanics*, **12**, 62.
- Ashour, M., Norris, G., and Pilling, P. (1998). "Lateral loading of a pile in layered soil using the strain wedge model." *Journal of Geotechnical and Geoenvironmental Engineering*, **124**, 303–315.
- Ashour, M., Norris, G.M., Elfass, S., and Al-Hamdan, A.Z. (2010). "Mobilized side and tip resistances of piles in clay." *Computers and Geotechnics*, **37**(7), 858–866.
- Chan, W., Chow, Y., and Liu, L. (1995). "Neural network: An alternative to pile driving formulas." *Computers and Geotechnics*, **17**(2), 135–156.
- Cho, S.E. (2009). "Probabilistic stability analyses of slopes using the ANN-based response surface." *Computers and Geotechnics*, **36**(5), 787–797.
- Das, B. (1995). *Principles of Foundation Engineering. PWS-KENT Series in Engineering*. 3rd Ed. PWS Publishing Company, Boston, Massachusetts.
- Das, S.K. and Basudhar, P.K. (2006). "Undrained lateral load capacity of piles in clay using artificial neural network." *Computers and Geotechnics*, **33**(8), 454–459.
- Ellis, G., Yao, C., Zhao, R., and Penumadu, D. (1995). "Stress-strain modeling of sands using artificial neural networks." *Journal of Geotechnical Engineering*, **121**(5), 429–435.
- Evans, L.T. (1982). *Simplified Analysis of Laterally Loaded Piles*. Report No. UCB/GT/82-04, University of California, Berkeley.
- Garrett, J. (1994). "Where and why artificial neural networks are applicable in civil engineering." *Journal of Computing in Civil Engineering*, ASCE, **8**, 129–130.
- Goh, A.T. (1996). "Pile driving records reanalyzed using neural networks." *Journal of Geotechnical Engineering*, **122**(6), 492–495.
- Goh, A.T. (2002). "Probabilistic neural network for evaluating seismic liquefaction potential." *Canadian Geotechnical Journal*, **39**(1), 219–232.
- Hornik, K., Stinchcombe, M., and White, H. (1989). "Multilayer feedforward networks are universal approximators." *Neural Networks*, **2**(5), 359–366.
- Javadi, A.A., Rezaei, M., and Nezhad, M.M. (2006). "Evaluation of liquefaction induced lateral displacements using genetic programming." *Computers and Geotechnics*, **33**(4), 222–233.
- Jeffreys, H. (1939). *Theory of Probability*. Oxford University Press.
- Kiefa, M.A. (1998). "General regression neural networks for driven piles in cohesionless soils." *Journal of Geotechnical and Geoenvironmental Engineering*, **124**(12), 1177–1185.
- Lahmiri, S. (2011). "A comparative study of backpropagation algorithms in financial prediction." *International Journal of Computational Science Engineering and Applications*, **1**(4), 15–21.
- Lee, J.-S. and Park, Y.-H. (2008). "Equivalent pile load-head settlement curve using a bi-directional pile load test." *Computers and Geotechnics*, **35**(2), 124–133.
- Levenberg, K. (1944). "A method for the solution of certain problems in least squares." *Quarterly of Applied Mathematics*, **2**, 164–168.
- Marquardt, D.W. (1963). "An algorithm for least-squares estimation of nonlinear parameters." *Journal of the Society for Industrial & Applied Mathematics*, **11**(2), 431–441.
- MATLAB (2014). *Version 8.3. 0.532 (R2014a)*. The Mathworks, Inc., Natick, Massachusetts.
- Millar, D.L. and Calderbank, P.A. (1995). "On the investigation of a multilayer feedforward neural network model of rock deformability behavior." *8th ISRM Congress*, International Society for Rock Mechanics.
- Momeni, E., Nazir, R., Armaghani, D.J., and Maizir, H. (2015). "Application of artificial neural network for predicting shaft and tip resistances of concrete piles." *Earth Sciences Research Journal*, **19**(1), 85–93.
- Motamed, R., Stanton, K., Elfass, S., and Kluzniak, B. (2016). *Development of the Nevada Deep Foundations Load Test Database: Drilled Shaft Component*. Number 16-3925, TRB, Washington D.C.
- Najjar, Y., Basheer, I., and McReynolds, R. (1996). "Neural modeling of Kansas soil swelling." *Transportation Research Record: Journal of the Transportation Research Board*, **1526**, 14–19.

- Nawari, N., Liang, R., and Nusairat, J. (1999). "Artificial intelligence techniques for the design and analysis of deep foundations." *Electronic Journal of Geotechnical Engineering*, **4**, 1–21.
- Neaupane, K.M. and Achet, S.H. (2004). "Use of backpropagation neural network for landslide monitoring: A case study in the higher himalaya." *Engineering Geology*, **74**(3), 213–226.
- Nejad, F.P., Jaksa, M.B., Kakhi, M., and McCabe, B.A. (2009). "Prediction of pile settlement using artificial neural networks based on standard penetration test data." *Computers and Geotechnics*, **36**(7), 1125–1133.
- Ni, S., Lu, P., and Juang, C. (1996). "A fuzzy neural network approach to evaluation of slope failure potential." *Computer-Aided Civil and Infrastructure Engineering*, **11**(1), 59–66.
- Norris, G. (1986). "Theoretically based BEF laterally loaded pile analysis." *Proceedings of the 3rd International Conference on Numerical Methods in Offshore Piling*, 361–386.
- O'Neill, M., Townsend, F., Hassan, K., Buller, A., and Chan, P. (1996). *Load Transfer for Drilled Shafts in Intermediate Geomaterials*. Report No. FHWA-RD-95-171, Federal Highway Administration.
- Ozer, M., Isik, N.S., and Orhan, M. (2008). "Statistical and neural network assessment of the compression index of clay-bearing soils." *Bulletin of Engineering Geology and the Environment*, **67**(4), 537–545.
- Padmini, D., Ilamparuthi, K., and Sudheer, K. (2008). "Ultimate bearing capacity prediction of shallow foundations on cohesionless soils using neurofuzzy models." *Computers and Geotechnics*, **35**(1), 33–46.
- Park, H. and Cho, C. (2010). "Neural network model for predicting the resistance of driven piles." *Marine Georesources and Geotechnology*, **28**(4), 324–344.
- Park, H. and Kim, Y. (2011). "Prediction of strength of reinforced lightweight soil using an artificial neural network." *Engineering Computations*, **28**(5), 600–615.
- Park, H., Kweon, G., and Lee, S. (2009). "Prediction of resilient modulus of granular subgrade soils and subbase materials using artificial neural network." *Road Materials and Pavement Design*, **10**(3), 647–665.
- Penumadu, D. and Zhao, R. (1999). "Triaxial compression behavior of sand and gravel using artificial neural networks (ANN)." *Computers and Geotechnics*, **24**(3), 207–230.
- Poulos, H.G. and Davis, E.H. (1980). *Pile Foundation Analysis and Design*. Wiley.
- Provenzano, P., Ferlisi, S., and Musso, A. (2004). "Interpretation of a model footing response through an adaptive neural fuzzy inference system." *Computers and Geotechnics*, **31**(3), 251–266.
- Reese, L. and O'Neill, M.W. (1988). *Drilled Shafts: Construction Procedures and Design Methods*. Prepared for US Department of Transportation, Federal Highway Administration, Office of Implementation.
- Reese, L.C., Wang, S.T., and Arrellaga, J.A. (2012). *A Program for the Study of Drilled Shafts Under Axial Loads*. Report No. SHAFT Version 2012 for Windows, Austin, Texas.
- Rinne, E., Thompson, J., and Vanderpool, W. (1996). *I-15/US 95 Load Test Program, Las Vegas, Nevada*. Report No. 31-215903-07A, Parsons Brinckerhoff, Las Vegas, Nevada.
- Rumelhart, D.E., Hinton, G.E., and Williams, R.J. (1988). "Learning representations by back-propagating errors." *Cognitive Modeling*, **5**, 3.
- Shahin, M., Jaksa, M., and Maier, H. (2005). "Stochastic simulation of settlement prediction of shallow foundations based on a deterministic artificial neural network model." *16th International Congress on Modelling and Simulation*, Melbourne, Victoria.
- Sidarta, D. and Ghaboussi, J. (1998). "Constitutive modeling of geomaterials from non-uniform material tests." *Computers and Geotechnics*, **22**(1), 53–71.
- Sivakugan, N., Eckersley, J., and Li, H. (1998). "Settlement predictions using neural networks." *Australian Civil Engineering Transactions*, **40**, 49.
- Stone, R.C. (2009). *Analysis of a Caliche Stiff d Pile Foundation*. Ph.D. Dissertation, University of Nevada, Las Vegas.
- Teh, C., Wong, K., Goh, A., and Jaritngam, S. (1997). "Prediction of pile capacity using neural networks." *Journal of Computing in Civil Engineering*, **11**(2), 129–138.
- Vesic, A. (1977). *Design of Pile Foundations, National Cooperative Highway Research Program Synthesis of Practice No. 42*. TRB, Washington, DC, 32–48.
- Western Technologies Inc. (1994). *Geotechnical Exploration, Fremont Street Experience*. Report No. Project No. 4123JZ254, Las Vegas, Nevada.
- Zadeh, L.A. (1965). "Fuzzy sets." *Information and Control*, **8**(3), 338–353.
- Zhao, H.-B. (2008). "Slope reliability analysis using a support vector machine." *Computers and Geotechnics*, **35**(3), 459–467.
- Zhu, J.-H., Zaman, M.M., and Anderson, S.A. (1998). "Modeling of soil behavior with a recurrent neural network." *Canadian Geotechnical Journal*, **35**(5), 858–872.